Insight through Molecular Mechanics Poisson−Boltzmann Surface Area Calculations into the Binding Affinity of Triclosan and Three Analogues for FabI, the *E. coli* Enoyl Reductase

Salma B. Rafi,[§,⊥] Guanglei Cui,[‡] Kun Song,[‡] Xiaolin Cheng,[‡] Peter J. Tonge,[‡,⊥] and Carlos Simmerling*[,‡,§,#,⊥]

Biochemistry and Structural Biology Graduate Program, Department of Chemistry, and Center for Structural Biology, Stony Brook University, New York 11794-5115, and Computational Science Center, Brookhaven National Laboratory, Upton, New York 11973

Received February 25, 2006

Keeping pace with emerging drug resistance in clinically important pathogens will be greatly aided by inexpensive yet reliable computational methods that predict the binding affinities of ligands for drug targets. We present results using the molecular mechanics Poisson−Boltzmann surface area (MM-PBSA) method to calculate the affinity of a series of triclosan analogues for the *E. coli* enoyl reductase FabI, spanning a 450000-fold range of binding affinities. Significantly, a high correlation is observed between the calculated binding energies and those determined experimentally. Further examination indicates that the van der Waals energies are the most correlated component of the total affinity ($r^2 = 0.74$), indicating that the shape of the inhibitor is very important in defining the binding energies for this system. The validation of MM-PBSA for the *E coli* FabI system serves as a platform for inhibitor design efforts focused on the homologous enzyme in *Staphylococcus aureues* and *Mycobacterium tuberculosis*.

Introduction

There is a compelling need for the development of new therapeutics, especially against unexploited drug targets, that are effective against drug-resistant strains of medically important pathogens. A promising target is the fatty acid synthase (FAS[a]) pathway in bacteria. Fatty acid biosynthesis is a fundamental and vital component of cellular metabolism and provides the building blocks for the formation of the bacterial cell wall. The bacterial fatty acid synthase system (FAS-II) is very different from that of yeast or animal fatty acid synthase system (FAS-I) with respect to the structural organization. The enzymes involved in FAS-II are monofunctional discrete proteins, while FAS-I contains all required enzymes in a single polypeptide chain, resulting in a multifunctional unit.[1−3] Because of its vital role and the organizational differences with its mammalian counterpart, the FAS-II system has become an attractive target for drug discovery efforts.[4]

The *E.coli* FAS-II pathway has been extensively studied[1] (Scheme 1). Successive rounds of elongation involve the addition of two carbons to the growing fatty acid from malonyl CoA followed by sequential condensation, reduction, dehydration, and reduction steps. Both the condensing enzymes and terminal reductases have previously been the focus of inhibitor design efforts. Thiolactomycin[5] and cerulenein inhibit the condensing enzymes,[6] while a variety of inhibitors have been developed that target the enoyl reductase FabI.[7] The diazaborine class of compounds are an early example of FabI inhibitors,[8] while the antituberculosis drug isonaizid (INH)[9,10] inhibits the FabI homologue in *Mycobacterium tuberculosis* (InhA). More recently it has been shown that the nonspecific biocide triclosan inhibits the FabI enzymes from a variety of organisms.[11] Initial SAR studies on the interaction of triclosan with FabI utilized analogues such as 2,2′-dihydroxy diphenyl ether, 2,2′-dihydroxy diphenyl thioether, and 2-hydroxy-3-phenoxybenzaldehyde, which have been studied as potent FabI inhibitors.[12]

Triclosan is effective against many pathogenic organisms, such as *Plasmodium falciparum*[13] and *Staphylococcus aureus*,[14] via inhibition of the FabI enzyme. While triclosan also inhibits InhA, the enoyl reductase from *Mycobacterium tuberculosis*,[15] the K_i for the inhibition is only 0.2 μM. Thus, triclosan is a promising lead compound for the development of potent InhA inhibitors, and a goal of the present studies is to develop methods that will be useful for rational modification of triclosan in order to improve binding affinity for InhA.

Computation can play an important role in lead compound optimization by predicting structural changes that will improve the affinity of inhibitors for their target enzymes. Several approaches exist, such as free energy perturbation (FEP), thermodynamic integration (TI), molecular mechanics Poisson−Boltzmann surface area (MM-PBSA),[16] and molecular mechanics generalized Born surface area (MM-GBSA).[17] The more recent MM-PBSA approach has been well studied[18,19] and used with success on many protein/ligand systems, such as avidin,[20] HIV reverse transcriptase,[21] neuraminidase,[22] cathepsin D,[23] Sem-5,[24] growth factor receptor binding protein 2,[25] and matrix metalloproteases.[26] MM-PBSA is advantageous in that it can be used for many types of intermolecular complexes and that it is "universal" and does not require fitting of additional parameters; however, it is rather time-consuming (although much less so than FEP or TI) and in some cases fails to accurately rank ligands. This may arise from approximations inherent in MM-PBSA, which will be discussed in more detail below. In particular, explicit water molecules are employed during molecular dynamics simulations but subsequently replaced with a continuum water model for evaluation of binding affinities.

To validate the use of the MM-PBSA method for the development of improved InhA inhibitors, we report its use in calculating relative binding affinities to FabI for a series of triclosan analogues. Experimental binding affinities for this triclosan analogue series have been published previously where it has been shown that small structural changes have a dramatic

* To whom correspondence should be addressed. Phone: 631-632-1336. Fax: 631-631-1555. E-mail: carlos.simmerling@stonybrook.edu.
⊥ Biochemistry and Structural Biology Graduation Program.
§ Center for Structural Biology, Stony Brook University.
‡ Department of Chemistry, Stony Brook University.
# Brookhaven National Laboratory.
[a] Abbreviations: FAS, fatty acid synthase; INH, isoniazid; CPP, 5-chloro-2-phenoxyphenol; FPP, 5-fluoro-2-phenoxyphenol; PP, 2-phenoxyphenol.

10.1021/jm060222t CCC: $33.50
Published on Web 07/06/2006

Scheme 1. Type II Fatty Acid Biosynthesis Pathway and FabI Inhibitors

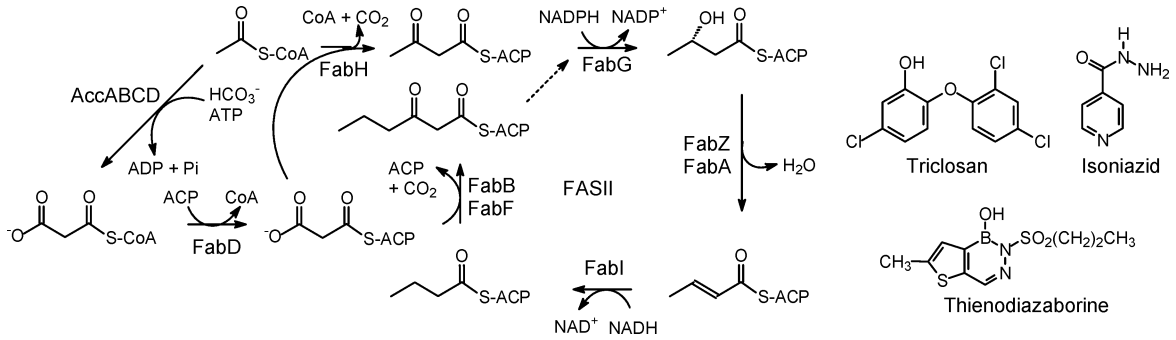

Table 1. Inhibition Data[a] for Triclosan and Three Diphenyl Ether Triclosan Analogues Binding to FabI

Name	Chemical structure	K_I with FabI
Triclosan	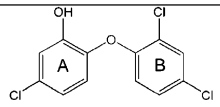 2-(2,4-dichlorophenoxy)-5-chlorophenol	**7.0 pM**
CPP	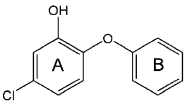 5-chloro-2-phenoxyphenol	**1.1 pM**
FPP	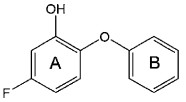 5-fluoro-2-phenoxyphenol	**1.5nM**
PP	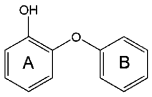 2-phenoxyphenol	**0.5 μM**

[a] K_I is the dissociation constant of the inhibitor from the enzyme/NAD^+ product complex. Data are taken from ref 27.

effect on affinity for FabI.[27] While removal of the triclosan B ring chlorine atoms has only a small effect on binding to FabI, removal of the A ring chlorine results in a 450000-fold decrease in affinity (Table 1). In addition, replacement of the A ring chlorine with methyl or fluoro substituents also has a dramatic effect on binding. Importantly, we show that the MM-PBSA approach results in excellent reproduction of the experimental data, with a correlation coefficient of 0.98 between computational and experimental relative affinities. Further analysis suggests that van der Waals energies are largely responsible for the variation in FabI affinity among the inhibitors. This in turn could be because of the changes in the cofactor conformation, and we note that the internal hydrogen bond in NAD^+ observed in the FabI/NAD^+/triclosan complex is mediated by a water molecule in the other FabI/NAD^+/inhibitor systems.

Methods

System Preparation. The crystal structure of the FabI/NAD^+/triclosan complex (1QSG)[28] was used to build the starting structures for the ternary complex with each of the triclosan analogues. This is a reasonable approach because these inhibitors all share the same scaffold and change only the identity of individual atoms on the phenyl rings that cannot act as a hydrogen bond donors or acceptors. We make the assumption that any small changes to the binding mode can be sampled during the molecular dynamics simulations. This is the typical approach used when only a single crystal structure is available for a series of highly related ligands.

Although FabI is a tetramer in solution, a fragment with a single binding site was generated in order to reduce computational cost. The fragment included all residues within 20 Å of triclosan in the complex, including 246 residues from this monomer and 115 amino acid residues from neighboring monomers. In the fragment system, all atoms beyond 15 Å from triclosan were weakly restrained with a 0.5 kcal/ (mol·Å) force constant. Three additional systems were built in a similar fashion using the FabI/NAD^+/triclosan structure as the template, with the assumption that triclosan and the three analogues are similar in shape and hence their binding mode to FabI will be similar to that of triclosan. Thus, for each system, the triclosan was replaced by the analogue (CPP, PP, or FPP) using the same coordinates for common atoms. Missing atoms were built using the LEAP module of Amber.

Each of the systems was then solvated in a truncated octahedral box of TIP3P water[29] with an 8 Å buffer between the solute and box edge, resulting in a system with 7262 water molecules and ∼27 000 atoms in total. Counterions were not used in any calculations. For each system, a total of 500 ps of molecular dynamics (MD) simulation at 300 K, with a constant pressure of 1 atm, periodic boundary conditions, and particle mesh Ewald[30,31] treatment of electrostatics, were performed with a time step of 1 fs. Snapshots were saved every 1 ps, yielding a total of 500 frames. The first 50 ps of data were regarded as equilibration and not used in the binding affinity analysis.

Force Field Parameters. Standard Amber ff99 force field parameters[32] were assigned to the protein. Triclosan and the analogues were parametrized as follows. The initial geometry of triclosan was obtained from the crystal structure of the FabI/NAD^+/triclosan complex (PDB code: 1QSG[28]); the triclosan analogues were created through manual modification of the triclosan structure. Each structure was optimized using Gaussian 98[33] at HF/6-31G*, and partial atomic charges (Tables S1−S4) were derived with standard RESP methodology.[34−36] To obtain the torsion angle parameters for the diphenyl ether linkage (Table S5), a potential energy scan (PES) was performed on these two angles with 36° intervals, and each of the resulting 100 geometries was optimized at RHF/6-31G* followed by calculation of single-point energies using MP2/6-31G*. These methods and basis set were chosen to be consistent with the procedure used in development of ff99. The quantum mechanics and molecular mechanics energy differences were calculated for each conformer, and the torsion angle Fourier series parameters were obtained using multivariate least-squares fitting. These parameters were developed on triclosan and used for all analogues.

MM-PBSA Calculations. MM-PBSA was used to calculate the relative binding free energies of triclosan and its analogues to the FabI fragment. The details of this method have been presented elsewhere.[19] Briefly, the binding affinity for a protein/ligand complex corresponds to the free energy of association in solution as shown in

$$\Delta G_{\text{bind}} = G_{\text{complex}} - (G_{\text{unbound protein}} + G_{\text{free ligand}}) \quad (1)$$

while the relative affinities for two ligands can be calculated using

$$\Delta\Delta G_{\text{bind}(1\rightarrow 2)} = \Delta G_{\text{bind}(2)} - \Delta G_{\text{bind}(1)} \quad (2)$$

In MM-PBSA, the binding affinity in eq 1 is typically calculated using

$$\Delta G_{\text{bind}} = \Delta E_{\text{MM}} + \Delta G_{\text{solv}} - T\Delta S_{\text{solute}} \quad (3)$$

where ΔE_{MM} represents the change in molecular mechanics potential energy upon formation of the complex, calculated using all bonded and nonbonded interactions. Solvation free energy, G_{solv}, is composed of the electrostatic component (G_{PB}) and a nonpolar component (G_{np}):

$$\Delta G_{\text{solv}} = \Delta G_{\text{PB}} + \Delta G_{\text{np}} \quad (4)$$

G_{PB} was calculated using the DelPhi program[37] with PARSE radii.[38] The cubic lattice had a grid spacing of 0.5 Å. Dielectric constants of 1 and 80 were used for the interior and exterior, respectively, and 1000 linear iterations were performed. The hydrophobic contribution to the solvation free energy, G_{np}, was calculated using the solvent accessible surface area (SASA)[38] from the MSMS program,[39] where $\gamma = 0.005\ 42$ kcal/(mol·Å^2) and $\beta = 0.92$ kcal/mol with a solvent probe radius of 1.4 Å:

$$\Delta G_{\text{np}} = \gamma\ \text{SASA} + \beta \quad (5)$$

$T\Delta S_{\text{solute}}$ represents the entropic contribution to binding affinity at temperature T. The four ligands used in these calculations are triclosan and three structurally very similar analogues. For a series of compounds with similar structures and binding modes, the entropy contribution can be omitted if one is only interested in relative binding affinities.[21,40] Since this calculation converges slowly and can have large uncertainties, we omitted the entropic contribution to $\Delta\Delta G$. The calculated error bars are standard errors (SE):

$$\text{SE} = \frac{\text{standard deviation}}{\sqrt{N}}$$

where N is the number of trajectory snapshots used in the calculations.

Results and Discussion

Despite spanning a range of 10^6 in dissociation constants, the diphenyl ether FabI inhibitors in Table 1 are structurally similar. All have a hydroxyl group on the A ring. Triclosan has a chlorine meta to the hydroxyl group on the A ring and two chlorine atoms on the B ring. Replacement of the B ring chlorines with hydrogens results in CPP, which, experimentally, is a 7-fold better inhibitor of FabI than triclosan[27] (Table 1). In contrast, replacement of the A ring chlorine in CPP with fluorine (FPP) results in a dramatic change in binding affinity, and experimentally FPP binds 1300-fold less tightly to FabI than CPP. Similarly, replacement of the fluorine with a hydrogen to give PP results in another large decrease in binding affinity and, overall, PP binds 450000-fold less tightly to FabI than CPP.

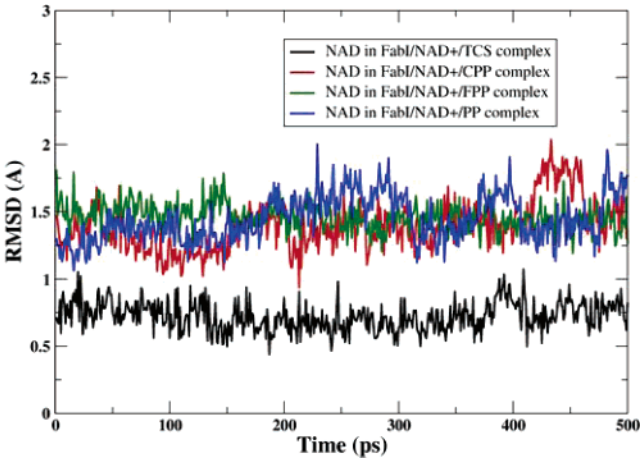

Figure 1. The rmsd vs time plot for NAD$^+$ in the FabI/NAD+/inhibitor simulations. The rmsd values were calculated between the position of NAD$^+$ during the simulation and the position of NAD$^+$ in the FabI/NAD$^+$/triclosan crystal structure. For the FabI/NAD$^+$/triclosan system, the rmsd of NAD$^+$ (black) is notably lower (<1 Å) than those for the FabI/NAD$^+$/CPP (red), FabI/NAD$^+$/FPP(green), and FabI/NAD$^+$/PP(blue) systems.

An important validation of the MM-PBSA approach to future ligand design efforts is to reproduce the experimental changes in binding affinity that occur as the triclosan skeleton is modified. In particular, the method should reproduce the high sensitivity to the substituent at the meta position on the A ring and the relative insensitivity to removal of the chlorine atoms on the B ring.

Molecular Dynamics Simulations. During the course of the MD simulations, the protein fragment was quite stable (<1 Å rmsd, data not shown). This and all other structural comparisons and rmsd values are reported with respect to the crystal structure of the FabI/NAD$^+$/triclosan ternary complex (PDB code: 1QSG[28]). The low rmsd likely reflects the use of positional restraints on atoms farther than 15 Å from the inhibitor. Neither the ligands nor the NAD$^+$ was restrained in any of the simulations. The rmsd of the inhibitors remained low (<2 Å, data not shown) and did not vary significantly between the different analogues. Interestingly, the rmsd values for the NAD$^+$ in the ternary complex did vary between the systems; the rmsd is in the range 0.5−1.0 Å with triclosan but is notably higher (1−2 Å) for the other analogues (Figure 1). Since the rmsd is low for the triclosan inhibitor that was used to obtain the crystal structure, it seems unlikely that the higher rmsd values that we observe for the other analogues arise solely from the simulation protocol or inaccuracies in the potential function. Instead, it is possible that the conformation of the NAD$^+$ indeed differs when the B ring chlorine atoms are removed. This may have implications for the binding affinity of the ligands and is discussed in more detail below.

To obtain an atomic-detail view of the changes that are reflected in these rmsd values, cluster analysis was performed on the four trajectories. In Figure 2, the representative structures for the inhibitor, NAD$^+$, and selected active site residues are compared to the experimentally determined structure of the FabI/NAD+/triclosan ternary complex. Consistent with the low rmsd values shown above, the structure of the complex obtained with triclosan reproduces the crystallographic data (Figure 2A) with an rmsd of ~0.75 Å for NAD$^+$ and ~1 Å for triclosan, again suggesting that the simulations can adequately reproduce the experimental structure data for this inhibitor. In contrast, the

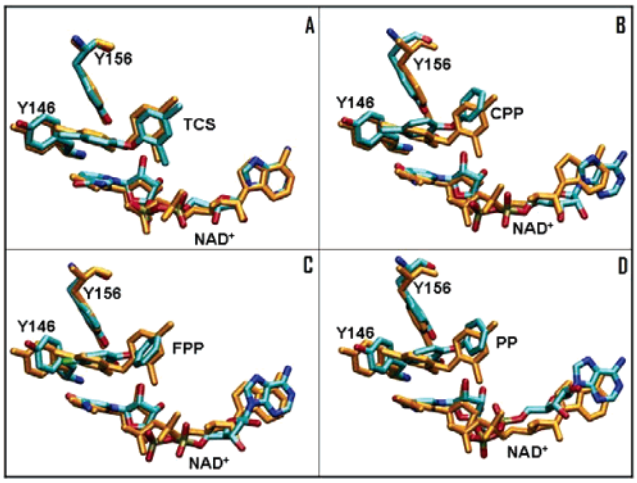

Figure 2. Comparison of the theoretical and experimental active site structures for the enzyme/inhibitor systems. The active sites of the four FabI/NAD^+/inhibitor systems from simulations (cyan/blue/red): (A) FabI/NAD^+/triclosan; (B) FabI/NAD^+/CPP; (C) FabI/NAD^+/FPP; (D) FabI/NAD^+/PP. For comparison, the crystal structure of the FabI/NAD^+/triclosan complex is shown in orange. For clarity, only heavy atoms are shown for the simulated systems.

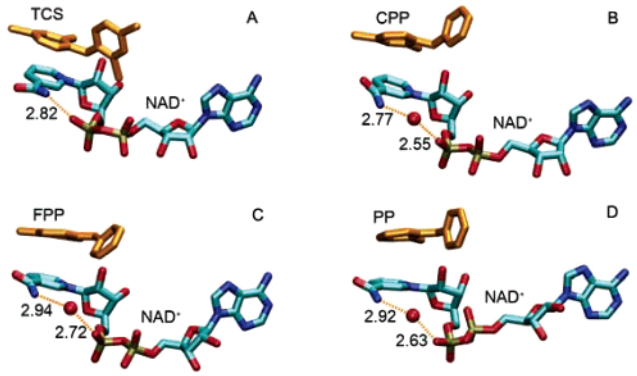

Figure 3. Bridging water molecule in the NAD^+ of the CPP, FPP, and PP complexes. Calculated structures showing the presence of a bridging water molecule (red atom) between the NAD^+ carboxamide and phosphate groups in the CPP, FPP, and PP complexes. The inhibitors are shown in orange: (A) FabI/NAD^+/triclosan; (B) FabI/NAD^+/CPP; (C) FabI/NAD^+/FPP; (D) FabI/NAD^+/PP. Consistent with the crystal structure, an intramolecular hydrogen bond is observed between the NAD^+ carboxamide and phosphate groups in the triclosan complex. When the inhibitor B ring chlorine atoms are removed (B−D), the intramolecular hydrogen bond is replaced by a water molecule.

complexes with the other three inhibitors show more significant differences from the triclosan complex (parts B−D of Figure 2) with ∼1.5 Å rmsd for NAD^+ and ∼2 Å for inhibitors. The close match between the simulated and experimental structures obtained with triclosan and the difference between the simulated structures for triclosan and the other analogues again suggest that the B ring chlorines play a role in the details of the NAD^+ conformation.

A comparison of the crystal structure of the FabI/NAD^+/triclosan complex to representative structures obtained by cluster analysis of the four simulations in explicit solvent reveals that the intramolecular hydrogen bond between the phosphate and the NH of the carboxamide group in the NAD^+ of the FabI/NAD^+/triclosan system (Figure 3A) is replaced by one bridging water molecule in the CPP, FPP, and PP systems (parts B−D of Figure 3).

Comparison of Calculated and Experimental Binding Affinities. The stability of the structures in the simulations and the close reproduction of the experimental binding mode for triclosan suggest that it is reasonable to use the simulation data for further analysis. The binding free energies calculated using the MM-PBSA approach are compared with the experimental free energies of binding[27] (absolute affinities, Table 2; relative affinities for all inhibitor pairs, Table 3). The MM-PBSA data reasonably reproduce the experimental absolute binding free energies, with an overall correlation coefficient of 0.85. The error for triclosan is <2 kcal/mol and is somewhat larger (3−4 kcal/mol) for the other inhibitors (Table 2). These differences in absolute affinities are quite reasonable given the approximations that were made in the simulations; the entropic component was neglected, and conformational change in the ligand and/or receptor upon binding was also neglected because of our use of a single trajectory for the bound and free states. It is likely that these effects are similar for each inhibitor and thus will largely cancel in the relative affinities. It is also possible that the removal of all of the water in the MM-PBSA calculation resulted in the increased error for CPP, FPP, and PP, each of which has a structured water molecule forming a hydrogen-bonding bridge in the NAD^+ cofactor (Figure 3). Since the triclosan-bound complex does not have this water molecule present, it would be difficult to include this effect in a straightforward manner in the MM-PBSA calculations.

The calculated absolute affinities indicate decreasing affinity for FabI in the order trilcosan, CPP, FPP, and PP. This rank order matches the experimental trends with the exception that the order of triclosan and CPP is reversed, with CPP binding more tightly than triclosan in the experimental data. This may again reflect error in MM-PBSA energies introduced by removal of the structured water in CPP that was not present in the triclosan complex. However, the simulation is in agreement with experiment in that the effect arising from removal of both B ring chlorines (TCS → CPP) is much smaller than the effects arising from removal of the A ring chlorine among the other inhibitors. For example, CPP and TCS differ by 2 kcal/mol in simulations and by 1.1 kcal/mol in experiment, while CPP and PP differ by 6.4 kcal/mol in simulation and by 7.7 kcal/mol in experiment.

Table 2 also shows the individual energy components contributing to the total calculated absolute binding free energies. It is interesting to note that the correlation with the total ΔG_{expt} is nearly zero for the ΔG_{polar} term, indicating that differences in desolvation of the inhibitor and enzyme upon binding are not directly responsible for the large variation in binding affinities of these analogues. Likewise, the correlation with the Coulomb electrostatic energies is quite poor ($r^2 = 0.3$). Although the correlation with the $\Delta G_{nonpolar}$(SASA) term is better ($r^2 = 0.5$), this term varies by only a few tenths of kcal/mol between the inhibitors.

Adding together the Coulomb and solvation terms does not improve the correlation ($r^2 = 0.03$), although this sum is large and positive for all of the inhibitors (20 to 25 kcal/mol), suggesting that the favorable electrostatic interactions between inhibitor and enzyme (−10 to −15 kcal/mol) are insufficient to completely overcome the large desolvation penalties (35 to 40 kcal/mol).

The van der Waals component shows the highest correlation with experimental affinities ($r^2 = 0.6$), consistent with previous MM-PBSA studies that also showed high correlation between van der Waals components and experimental binding affinities.[24,41] Despite the low level of correlation for the Coulomb and solvation sum, adding it to the van der Waals term improves the quality of the fit, with an overall correlation coefficient of

Table 2. Individual Energy Components for the Calculated Absolute Binding Free Energies

system	ΔE_{vdw} ($N = 450$) A	ΔE_{coul} ($N = 450$) B	ΔG_{polar} ($N = 450$) C	$\Delta G_{nonpolar}$ ($N = 450$) D	$\Delta E_{electro}$ B + C + D	$\Delta G_{MM-PBSA}$ A + B + C + D	$\Delta G_{expt} = RT \ln(K_1)$
TCS	-37.28 ± 0.11	-11.70 ± 0.10	39.15 ± 0.15	-4.36 ± 0.01	23.09 ± 0.15	-14.19 ± 0.14	-15.46
CPP	-31.91 ± 0.12	-11.43 ± 0.09	35.11 ± 0.16	-3.98 ± 0.01	19.70 ± 0.15	-12.20 ± 0.13	-16.56
FPP	-29.30 ± 0.11	-9.73 ± 0.12	35.97 ± 0.30	-3.97 ± 0.01	22.27 ± 0.28	-7.03 ± 0.25	-11.76
PP	-27.10 ± 0.15	-10.92 ± 0.11	35.98 ± 0.37	-3.74 ± 0.01	21.32 ± 0.38	-5.78 ± 0.28	-8.73
	$r^2 = 0.63$	$r^2 = 0.31$	$r^2 = 0.05$	$r^2 = 0.50$	$r^2 = 0.03$	$r^2 = 0.85$	

Table 3. Individual Energy Components for the Calculated Relative Binding Free Energies

system	$\Delta\Delta E_{vdw}$ ($N = 450$) A	$\Delta\Delta E_{coul}$ ($N = 450$) B	$\Delta\Delta G_{polar}$ ($N = 450$) C	$\Delta\Delta G_{nonpolar}$ ($N = 450$) D	$\Delta\Delta E_{electro}$ B + C + D	$\Delta\Delta G_{MM-PBSA}$ A + B + C + D	$\Delta\Delta G_{expt} = RT \ln(K_1)$
a: PP−TCS	10.17 ± 0.17	0.78 ± 0.15	-3.16 ± 0.34	0.62 ± 0.01	-1.76 ± 0.37	8.41 ± 0.41	6.6
b: CPP−TCS	5.36 ± 0.15	0.27 ± 0.13	-4.03 ± 0.18	0.36 ± 0.01	-3.39 ± 0.19	1.99 ± 0.27	-1.1
c: FPP−TCS	7.98 ± 0.16	1.97 ± 0.15	-3.18 ± 0.36	0.39 ± 0.01	-0.82 ± 0.35	7.16 ± 0.42	3.6
d: CPP−PP	-4.80 ± 0.14	-0.51 ± 0.15	-0.87 ± 0.32	-0.25 ± 0.01	-1.63 ± 0.36	-6.42 ± 0.38	-7.7
e: FPP−PP	-2.20 ± 0.17	1.19 ± 0.17	-0.01 ± 0.44	-0.23 ± 0.01	0.95 ± 0.47	-1.25 ± 0.50	-3
f: FPP−CPP	2.60 ± 0.14	1.70 ± 0.15	0.86 ± 0.38	0.01 ± 0.01	2.56 ± 0.34	5.17 ± 0.43	4.7
	$r^2 = 0.74$	$r^2 = 0.49$	$r^2 = 0.047$	$r^2 = 0.56$	$r^2 = 0.051$	$r^2 = 0.96$	

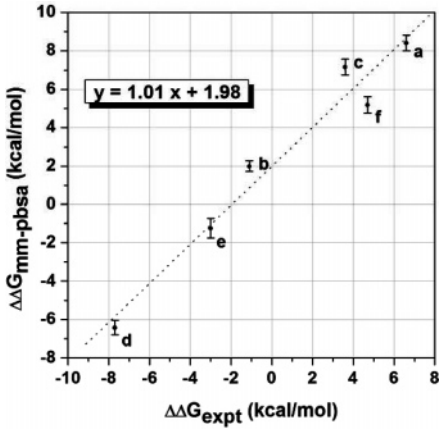

Figure 4. Correlation between the relative experimental and theoretical binding free energies. A high correlation and nearly linear slope is observed between relative binding free energies obtained experimentally and the binding energies calculated using the MM-PBSA approach: (a) PP−triclosan; (b) CPP−triclosan; (c) FPP−triclosan; (d) CPP−PP; (e) FPP−PP; (f) FPP−CPP.

0.85 for the total binding free energies. Overall, this suggests that the affinities of these inhibitors for FabI are dominated by shape complementarity, but the total affinity arises from a more complex interplay between all of these components.

These effects are more apparent when one examines the relative binding affinities between all six pairs of inhibitors (Figure 4). As expected, the correlation in the relative affinities is much improved, likely because of substantial cancellation of the errors arising from neglect of entropy and conformational changes in the enzyme in the absolute affinities. As shown in Figure 4 and Table 3, the relative binding affinities of the analogues show an impressive correlation coefficient of 0.98 between calculation and experiment. In addition, the slope of the best-fit line (obtained through linear regression) is 1.01, indicating not only that the data are well correlated but also that the differences in affinities are reproduced nearly quantitatively by the simulations.

As noted above, the sign of $\Delta\Delta G$ is incorrect for the triclosan−CPP pair; triclosan appears to bind 2−3 kcal/mol too strongly in all of the simulations compared to the analogues without the B ring chlorine atoms. A possible explanation for this discrepancy is the removal of the structured water molecule that forms the hydrogen bond bridge in the NAD^+ of the CPP, FPP, and PP complexes (Figure 3).

On the basis of the high correlation of the relative binding affinities with the experimental data, we further investigated which energy components were most correlated with the experimental relative affinities. All components contributing to each data point in Figure 4 are shown in Table 3. Similar to the absolute affinities, the van der Waals energies are well correlated ($r^2 = 0.74$) with the experimental values (which, of course, reflect all interactions). In addition, the van der Waals terms are the largest component of the *relative* affinity for each of the pairs. This indicates that the shape of the inhibitor plays an important role in defining the relative affinities of these inhibitors for FabI, much as the large magnitude of the van der Waals term in the total affinities suggested that this term was also the most important for defining the absolute affinity of each of the inhibitors. One might imagine that the interactions that give rise to strong binding need not be the same as those that discriminate among the inhibitors, but in the present case these arise from the same type of interaction. The $\Delta G_{nonpolar}$ term contributes less than 1 kcal/mol to each of the relative affinities, consistent with the small differences in solvent accessible surface area among the inhibitors. The sum of Coulomb and solvation terms shows little correlation, also consistent with our observations for the total affinities, but once again the addition of this term to the van der Waals component improves the quality of the fit (with r^2 increasing from 0.74 to 0.96 upon inclusion of electrostatic and desolvation effects).

Because of the importance of the van der Waals interactions not only in the absolute affinities but also in defining the relative binding of the analogues, we performed a further decomposition of this component into terms involving each amino acid in the enzyme. Our goal was to gain insight into specific active site residues that influence the relative affinities, with potential application in the design of improved inhibitors that optimize these key interactions. We considered separately the effects of changing substituents on the A ring (PP vs CPP) and B ring (triclosan vs CPP). The residues contributing significantly to the difference in binding are shown in Figure 5 with energy values in Table 4.

With respect to the difference in binding of CPP and triclosan, van der Waals interactions with the NAD^+ cofactor contribute ~3 of the total 5.3 kcal/mol. This is reasonable considering that

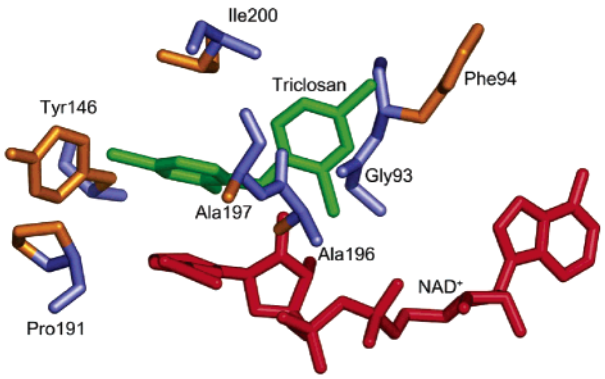

Figure 5. Active site cavity of FabI showing the position of triclosan, NAD^+, and selected active site residues: NAD^+, red; triclosan, green; backbone, blue; side chains, orange.

Table 4. Residues in FabI That Are Sensitive to Removal of the Triclosan Chlorine Atoms[a]

residue	$\Delta\Delta E_{vdw}$(TCS−CPP) (kcal/mol)	residue	$\Delta\Delta E_{vdw}$(CPP−PP) (kcal/mol)
Gly93	−0.81	Tyr146	−0.61
Phe94	−0.81	Pro191	−0.61
Ala196	−1.21	Ala196	0.85
Ala197	1.01	Ala197	−1.74
NAD^+	−2.97	Ile200	−0.52

[a] Residues that contribute more than 0.5 kcal/mol in van der Waals energies for removal of A ring (triclosan vs CPP) and B ring (CPP vs PP) chlorine atoms. Residues are shown in Figure 5.

the chlorine at the ortho position on the B ring is in direct contact with the NAD^+ phosphates in both the crystal structure and the simulations of the FabI/NAD^+/triclosan ternary complex. This contact may also play a role in stabilizing the observed position of the NAD^+ in the binding pocket, since all simulations with inhibitors that lacked B ring chlorines showed a change in the NAD^+ conformation (Figure 1). The other residues contributing significantly (greater than 0.5 kcal/mol) to the van der Waals binding energy difference for B ring chlorines (triclosan−CPP) are Gly93, Phe94, Ala196, and Ala197, residues that are all close to the B ring. Important residues for removal of the A ring chlorine are Tyr146, Pro191, Ala196, Ala197, and Ile200. Ala196 and Ala197 are in the substrate binding loop. Residues Gly93, Phe94, Tyr146, and Pro191 are a part of the active site pocket, with Tyr146 and Pro191 in proximity to the A ring (Figure 5).

Conclusions

We applied the computationally inexpensive MM-PBSA method to calculate the relative binding affinities of a series of inhibitors to FabI, the *E. coli* enoyl reductase enzyme. We used the crystal structure of the triclosan-bound ternary complex to generate the initial binding modes for the other analogues because they all share the same scaffold. The rank ordering of the calculated ligand affinities was correct with the exception of triclosan and CPP, the pair that represents the smallest difference in affinity in both simulation and experiment. Triclosan was found to bind somewhat too strongly relative to all of the other inhibitors (compared to experiment), possibly because of a difference in water structuring between triclosan and the other inhibitors that we observed in simulations. Incorporation of these effects into an implicit solvent model such as that used with MM-PBSA is nontrivial. In the present case it is particularly difficult because the water is well ordered in the complex containing CPP, FPP, and PP while it is disordered with TCS.

Overall, the binding free energy data obtained from MM-PBSA were in excellent quantitative agreement with experimental K_I data, with a correlation coefficient of 0.98 and a slope of 1.01. Particularly notable is that the calculations also reproduce the high sensitivity to removal of the chlorine atom on the triclosan A ring as well as the relative insensitivity to removal of the B ring chlorines. This high level of agreement validates the data and suggests that it is reasonable to further examine the specific interactions and energy components that influence binding. Energy decomposition analysis was performed to study the contribution of different interaction types toward the relative affinities. This showed that the van der Waals energies were most highly correlated to experimental data for both the absolute and relative affinities. In addition, the Coulomb electrostatic interaction between protein and inhibitor was observed to be insufficient to overcome the unfavorable desolvation energy. Adding together the Coulomb and solvation terms does not improve the correlation ($r^2 = 0.03$), although this sum is large and positive for all of the inhibitors (20−25 kcal/mol), suggesting a possible route to further optimization of affinity. Together, these imply that the shape of the ligand plays an important role in determining its binding affinity. This information will be of critical importance for designing more potent inhibitors of the homologous enzyme in *M. tuberculosis*.

Acknowledgment. C.S. thanks Rob Rizzo for helpful discussions. Financial support from NIH (Grant GM6167803) and DOE (Grant DE-AC02-98CH10886) and supercomputer time at NCSA (Grant NPACI MCA02N028) are gratefully acknowledged. C.S. is a Cottrell Scholar of Research Corporation.

Supporting Information Available: Tables of force field parameters for triclosan and analogues. This material is available free of charge via the Internet at http://pubs.acs.org.

References

(1) Cronon, J. E., Jr.; Rock, C. O., *Biosynthesis of Membrane Lipids in Escherichia coli* and *Salmonella typhimurium: Cellular and Molecular Biology*; American Society of Microbiology: Washington, DC, 1996; pp 612−636.
(2) Rock, C. O.; Jackowski, S. Forty years of bacterial fatty acid synthesis. *Biochem. Biophys. Res. Commun/* **2002**, *292* (5), 1155−1166.
(3) Rock, C. O.; Cronan, J. E. *Escherichia coli* as a model for the regulation of dissociable (type II) fatty acid biosynthesis. *Biochim. Biophys. Acta* **1996**, *1302* (1), 1−16.
(4) Zhang, Y. M.; Lu, Y. J.; Rock, C. O. The reductase steps of the type II fatty acid synthase as antimicrobial targets. *Lipids* **2004**, *39* (11), 1055−1060.
(5) Hayashi, T.; Yamamoto, O.; Sasaki, H.; Okazaki, H.; Kawaguchi, A. Inhibition of fatty acid synthesis by the antibiotic thiolactomycin. *J Antibiot. (Tokyo)* **1984**, *37* (11), 1456−1461.
(6) Price, A. C.; Choi, K. H.; Heath, R. J.; Li, Z.; White, S. W.; Rock, C. O. Inhibition of beta-ketoacyl-acyl carrier protein synthases by thiolactomycin and cerulenin. Structure and mechanism. *J. Biol. Chem.* **2001**, *276* (9), 6551−6559.
(7) Moir, D. T. Identification of inhibitors of bacterial enoyl-acyl carrier protein reductase. *Curr. Drug Targets: Infect. Disord.* **2005**, *5* (3), 297−305.
(8) Baldock, C.; Rafferty, J. B.; Sedelnikova, S. E.; Baker, P. J.; Stuitje, A. R.; Slabas, A. R.; Hawkes, T. R.; Rice, D. W. A mechanism of drug action revealed by structural studies of enoyl reductase. *Science* **1996**, *274* (5295), 2107−2110.
(9) Banerjee, A.; Dubnau, E.; Quemard, A.; Balasubramanian, V.; Um, K. S.; Wilson, T.; Collins, D.; de Lisle, G.; Jacobs, W. R., Jr. inhA, a gene encoding a target for isoniazid and ethionamide in *Mycobacterium tuberculosis*. *Science* **1994**, *263* (5144), 227−230.
(10) Rozwarski, D. A.; Grant, G. A.; Barton, D. H. R.; Jacobs, W. R., Jr.; Sacchettini, J. C. Modification of the NADH of the isoniazid target (InhA) from *Mycobacterium tuberculosis*. *Science* **1998**, *279* (5347), 98−102.

(11) McMurry, L. M.; Oethinger, M.; Levy, S. B. Triclosan targets lipid synthesis. *Nature* **1998**, *394* (6693), 531−532.
(12) Heath, R. J.; Yu, Y. T.; Shapiro, M. A.; Olson, E.; Rock, C. O. Broad spectrum antimicrobial biocides target the FabI component of fatty acid synthesis. *J. Biol. Chem.* **1998**, *273* (46), 30316−30320.
(13) Surolia, N.; Surolia, A. Triclosan offers protection against blood stages of malaria by inhibiting enoyl-ACP reductase of *Plasmodium falciparum*. *Nat. Med.* **2001**, *7* (5), 636−636 (erratum for *Nat. Med.* **2001**, *7* (5), 167−173).
(14) Heath, R. J.; Li, J.; Roland, G. E.; Rock, C. O. Inhibition of the *Staphylococcus aureus* NADPH-dependent enoyl-acyl carrier protein reductase by triclosan and hexachlorophene. *J. Biol. Chem.* **2000**, *275* (7), 4654−4659.
(15) Parikh, S. L.; Xiao, G.; Tonge, P. J. Inhibition of InhA, the enoyl-reductase from *Mycobacterium tuberculosis*, by triclosan and isoniazid. *Biochemistry* **2000**, *39* (26), 7645−7650.
(16) Srinivasan, J.; Cheatham, T. E.; Cieplak, P.; Kollman, P. A.; Case, D. A. Continuum solvent studies of the stability of DNA, RNA, and phosphoramidate−DNA helices. *J. Am. Chem. Soc.* **1998**, *120* (37), 9401−9409.
(17) Gohlke, H.; Kiel, C.; Case, D. A. Insights into protein−protein binding by binding free energy calculation and free energy decomposition for the Ras-Raf and Ras-RaIGDS complexes. *J. Mol. Biol.* **2003**, *330* (4), 891−913.
(18) Massova, I.; Kollman, P. A. Combined molecular mechanical and continuum solvent approach (MM-PBSA/GBSA) to predict ligand binding. *Perspect. Drug Discovery Des.* **2000**, *18*, 113−135.
(19) Kollman, P. A.; Massova, I.; Reyes, C.; Kuhn, B.; Huo, S.; Chong, L.; Lee, M.; Lee, T.; Duan, Y.; Wang, W.; Donini, O.; Cieplak, P.; Srinivasan, J.; Case, D. A.; Cheatham, T. E., 3rd. Calculating structures and free energies of complex molecules: combining molecular mechanics and continuum models. *Acc. Chem. Res.* **2000**, *33* (12), 889−897.
(20) Kuhn, B.; Kollman, P. A. Binding of a diverse set of ligands to avidin and streptavidin: An accurate quantitative prediction of their relative affinities by a combination of molecular mechanics and continuum solvent models. *J. Med. Chem.* **2000**, *43* (20), 3786−3791.
(21) Wang, J. M.; Morin, P.; Wang, W.; Kollman, P. A. Use of MM-PBSA in reproducing the binding free energies to HIV-1 RT of TIBO derivatives and predicting the binding mode to HIV-1 RT of efavirenz by docking and MM-PBSA. *J. Am. Chem. Soc.* **2001**, *123* (22), 5221−5230.
(22) Masukawa, K. M.; Kollman, P. A.; Kuntz, I. D. Investigation of neuraminidase-substrate recognition using molecular dynamics and free energy calculations. *J. Med. Chem.* **2003**, *46* (26), 5628−5637.
(23) Huo, S.; Wang, J.; Cieplak, P.; Kollman, P. A.; Kuntz, I. D. Molecular dynamics and free energy analyses of cathepsin D−inhibitor interactions: insight into structure-based ligand design. *J. Med. Chem.* **2002**, *45* (7), 1412−1419.
(24) Wang, W.; Lim, W. A.; Jakalian, A.; Wang, J.; Wang, J. M.; Luo, R.; Bayly, C. T.; Kollman, P. A. An analysis of the interactions between the Sem-5 SH3 domain and its ligands using molecular dynamics, free energy calculations, and sequence analysis. *J. Am. Chem. Soc.* **2001**, *123* (17), 3986−3994.
(25) Suenaga, A.; Hatakeyama, M.; Ichikawa, M.; Yu, X. M.; Futatsugi, N.; Narumi, T.; Fukui, K.; Terada, T.; Taiji, M.; Shirouzu, M.; Yokoyama, S.; Konagaya, A. Molecular dynamics, free energy, and SPR analyses of the interactions between the SH2 domain of grb2 and ErbB phosphotyrosyl peptides. *Biochemistry* **2003**, *42* (18), 5195−5200.
(26) Donini, O. A. T.; Kollman, P. A. Calculation and prediction of binding free energies for the matrix metalloproteinases. *J. Med. Chem.* **2000**, *43* (22), 4180−4188.
(27) Sivaraman, S.; Sullivan, T. J.; Johnson, F.; Novichenok, P.; Cui, G. L.; Simmerling, C.; Tonge, P. J. Inhibition of the bacterial enoyl reductase FabI by triclosan: A structure−reactivity analysis of FabI inhibition by triclosan analogues. *J. Med. Chem.* **2004**, *47* (3), 509−518.
(28) Stewart, M. J.; Parikh, S.; Xiao, G. P.; Tonge, P. J.; Kisker, C. Structural basis and mechanism of enoyl reductase inhibition by triclosan. *J. Mol. Biol.* **1999**, *290* (4), 859−865.
(29) Jorgensen, W. L.; Chandrasekhar, J.; Madura, J. D.; Impey, R. W.; Klein, M. L. Comparison of simple potential functions for simulating liquid water. *J. Chem. Phys.* **1983**, *79* (2), 926−935.
(30) Darden, T.; York, D.; Pedersen, L. Particle mesh Ewald, an N.Log(N) method for Ewald sums in large systems. *J. Chem. Phys.* **1993**, *98*, (12), 10089−10092.
(31) Petersen, H. G. Accuracy and efficiency of the particle mesh Ewald method. *J. Chem. Phys.* **1995**, *103* (9), 3668−3679.
(32) Wang, J. M.; Cieplak, P.; Kollman, P. A. How well does a restrained electrostatic potential (RESP) model perform in calculating conformational energies of organic and biological molecules? *J. Comput. Chem.* **2000**, *21* (12), 1049−1074.
(33) Frisch, M. J.; Trucks, G. W.; Schlegel, H. B.; Scuseria, G. E.; Robb, M. A.; Cheeseman, J. R.; Zakrzewski, V. G.; Montgomery, J. A., Jr.; Stratmann, R. E.; Burant, J. C.; Dapprich, S.; Millam, J. M.; Daniels, A. D.; Kudin, K. N.; Strain, M. C.; Farkas, O.; Tomasi, J.; Barone, V.; Cossi, M.; Cammi, R.; Mennucci, B.; Pomelli, C.; Adamo, C.; Clifford, S.; Ochterski, J.; Petersson, G. A.; Ayala, P. Y.; Cui, Q.; Morokuma, K.; Malick, D. K.; Rabuck, A. D.; Raghavachari, K.; Foresman, J. B.; Cioslowski, J.; Ortiz, J. V.; Stefanov, B. B.; Liu, G.; Liashenko, A.; Piskorz, P.; Komaromi, I.; Gomperts, R.; Martin, R. L.; Fox, D. J.; Keith, T.; Al-Laham, M. A.; Peng, C. Y.; Nanayakkara, A.; Gonzalez, C.; Challacombe, M.; Gill, P. M. W.; Johnson, B. G.; Chen, W.; Wong, M. W.; Andres, J. L.; Head-Gordon, M.; Replogle, E. S.; Pople, J. A. *Gaussian 98*, revision A.5; Gaussian, Inc.: Pittsburgh, PA, 1998.
(34) Cornell, W. D.; Cieplak, P.; Bayly, C. I.; Kollman, P. A. Application of Resp charges to calculate conformational energies, hydrogen-bond energies, and free-energies of solvation. *J. Am. Chem. Soc.* **1993**, *115* (21), 9620−9631.
(35) Bayly, C. I.; Cieplak, P.; Cornell, W. D.; Kollman, P. A. A well-behaved electrostatic potential based method using charge restraints for deriving atomic charges. The Resp model. *J. Phys. Chem.* **1993**, *97* (40), 10269−10280.
(36) Cieplak, P.; Cornell, W. D.; Bayly, C.; Kollman, P. A. Application of the multimolecule and multiconformational Resp methodology to biopolymers. Charge derivation for DNA, Rna, and proteins. *J. Comput. Chem.* **1995**, *16* (11), 1357−1377.
(37) Honig, B.; Nicholls, A. Classical electrostatics in biology and chemistry. *Science* **1995**, *268* (5214), 1144−1149.
(38) Sitkoff, D.; Sharp, K. A.; Honig, B. Accurate calculation of hydration free-energies using macroscopic solvent models. *J. Phys. Chem.* **1994**, *98* (7), 1978−1988.
(39) Sanner, M. F.; Olson, A. J.; Spehner, J. C. Reduced surface: An efficient way to compute molecular surfaces. *Biopolymers* **1996**, *38* (3), 305−320.
(40) Zhuang, S.; Zou, J.; Jiang, Y.; Mao, X.; Zhang, B.; Liu, H.; Yu, Q. Some insights into the stereochemistry of inhibition of macrophage migration inhibitory factor with 2-fluoro-*p*-hydroxycinnamate and its analogues from molecular dynamics simulations. *J. Med. Chem.* **2005**, *48*, 7208−7214.
(41) Rizzo, R. C.; Toba, S.; Kuntz, I. D. A molecular basis for the selectivity of thiadiazole urea inhibitors with stromelysin-1 and gelatinase-A from generalized Born molecular dynamics simulations. *J. Med. Chem.* **2004**, *47* (12), 3065−3074.

JM060222T